Journal of Materials Chemistry C

The Effect of Molecular Isomerism on the Induced Circular Dichroism of Cadmium Sulfide Quantum Dots

Journal:	*Journal of Materials Chemistry C*
Manuscript ID	TC-ART-09-2021-004496.R2
Article Type:	Paper
Date Submitted by the Author:	18-Nov-2021
Complete List of Authors:	Joh, Yoonbin; University of New Hampshire KWON, Yuri; University of New Hampshire College of Life Sciences and Agriculture, Molecular, Cellular, and Biomedical Sciences Tannir, Shambhavi; Boston University, Chemistry Leonard, Brian; University of Wyoming, Dept. of Chemistry Kubelka, Jan; University of Wyoming, Department of Chemistry Varga, Krisztina; University of New Hampshire Balaz, Milan; Yonsei University Underwood International College, Integrated Science and Engineering Division

ARTICLE

The Effect of Molecular Isomerism on the Induced Circular Dichroism of Cadmium Sulfide Quantum Dots

Received 00th January 20xx,
Accepted 00th January 20xx

DOI: 10.1039/x0xx00000x

Yoonbin A. Joh,[a] Yuri H. Kwon,[a] Shambhavi Tannir,[b †] Brian M. Leonard,[b] Jan Kubelka,[c] Krisztina Varga,[a*] and Milan Balaz[d*]

Post-synthetic phase transfer ligand exchange has been established as a simple, reliable, and versatile method for the synthesis of chiral, optically active colloidal nanocrystals displaying circular dichroism (CD) and circularly polarized luminescence (CPL). Herein we present a water-free and purification-free cyclohexane → methanol ligand exchange system that led to the synthesis of stable, non-aggregating chiral and fluorescent cadmium sulfide quantum dots (CdS QDs). Absorption and emission studies revealed that the carboxylate capping ligands can tune the band gap by up to 65 meV as well as control the band gap and deep trap emission pathways. The CD data revealed that the addition of a 2nd stereogenic center did not automatically lead to an increase of the CD anisotropy of QDs, but rather match/mismatch cooperativity effects must be considered in the transfer of the chirality from the capping ligands to the achiral nanocrystals. Variation in position of the functional groups as well as the chiral identity of the functional groups impacted both the shape and anisotropy of the induced CD spectra and revealed the importance of the functional groups' coordination and polarity on the binding geometry and induced chiroptical properties. Finally, we describe the first example where CD spectra of QDs capped with the same ligand and dissolved in the same solvent displayed very different spectral profiles. This work provides deeper insight into induced CD of QDs and paves the path to rational design of chiral nanomaterials.

1. Introduction

Capping ligands are organic molecules on the surface of the quantum dots (QDs) that stabilize colloidal QDs and can modify existing or induce new electronic, optical and chiroptical properties of QDs. First chiral QDs in the form of penicillamine capped CdS have been prepared by Gun'ko and coworkers by microwave-assisted aqueous synthesis from individual components in the presence of chiral ligands.[1, 2] We have later shown that chirality can be induced *de novo* in achiral and optically inactive QDs, as evidenced by appearance of circular dichroism (CD) or circularly polarized luminescence (CPL) signals,[3, 4] by post-synthetic replacement of the achiral ligands with chiral ligands. Post-synthetic ligand exchange has since been established as the method of choice for the synthesis of chiral QDs and has been successfully used for preparation of optically active core/shell nanocrystals, dot/rod nanocrystals, quantum rods and nanoplatelets.[5-8] Chiral QDs prepared by post-synthetic phase-transfer ligand exchange exhibited excellent structural and chiroptical properties and have been explored for a variety of applications including DNA and drug sensing, living cell biorecognition, asymmetric catalysis, CPL emitters, and spintronics.[9-19] Using a combination of spectroscopy and non-empirical, fully quantum chemical simulations, we have proposed that the induced CD signal is a result of hybridization of the achiral electronic states of QD and chiral electronic states of ligands. The observed induced CD signal is the result of an interplay of the following three factors: (i) the stereogenic information embedded in the ligand structure (ligand's absolute configuration), (ii) ligand's binding geometry (ligand's conformation), and (iii) ligands' topological relationship (binding pattern) on the surface of the QDs.[20, 21] Similarly, orbitals mixing of the chiral amino acids with graphene edges has been proposed as the origin of the chiroptical activity of cysteine functionalized graphene quantum dots by Kotov, Violi and coworkers.[22] The importance of binding geometry on the induced CD was further confirmed by Nakashima and coworkers who rationalized the temperature-induced inversion of CD signal of Ac-L-Cys capped HgS by "mirror-image" bidentate binding of the ligand on the surface of QDs (bidentate binding = capping ligand binds to the surface via two functional groups).[23] However, it is worth to note that the native achiral ligands used in the synthesis of QDs also play a role in the shape and anisotropy of the observed induced CD of QDs prepared by post-synthetic ligand exchange.[4, 24] Markovich, Oron and coworkers have showed that experimental CD spectrum of QDs could be rationalized as a sum of the different excitonic transitions originating from cysteine chiral ligand induced split of an exciton level into two

[a] *University of New Hampshire, Department of Molecular, Cellular, and Biomedical Sciences, Durham, NH, USA*
[b] *University of Wyoming, Department of Chemistry, Laramie, WY, USA.*
[c] *University of Wyoming, Department of Petroleum Engineering, Laramie, WY, USA*
[d] *Yonsei University, Underwood International College, Integrated Science and Engineering Division, Seoul, Republic of Korea*
† Current address: Department of Chemistry, Boston University, Boston, MA, USA.
Electronic Supplementary Information (ESI) available: The Supporting Information is available free of charge on the ACS Publications website at DOI: [UV-vis, emission, DLS, NMR, and FTIR data of chiral CdS QDs]. See DOI: 10.1039/x0xx00000x

new sublevels with opposite angular momentums.[25] Markovich[25] and Gun'ko[26] reported that the CD signal intensity of CdSe/CdS QDs decreased with shell thickness; a behavior again explained by the hybridization theory where the chirality originates from the hybridization of the energy level of the QD hole and HOMO level of the chiral molecules. Moreover, the cysteine concentration during the post-synthetic ligand exchange has been shown to impact intensity of CD and CPL spectra of core/shell QDs by impacting the ligand's binding mode (mono-, di- and tri-dentate), yet had little effect on the overall shape of the CD spectra.[6, 27] While the effect of chiral thiols (cysteine and its derivatives) on induced CD of QDs has been explored in detail, only few studies have focused on the chiroptical properties of QDs functionalized with chiral carboxylic acid ligands that do not contain sulfhydryl groups.[21, 28, 29] We have prepared water-soluble chiral carboxylic acid capped CdSe prepared by a toluene-water phase-transfer ligand exchange procedure, however only two chiral acids, malic acid and tartaric acid, induced CD in QDs in water, a polar protic solvent.[21] Subsequently, Ferry and coworker[28] reported chiral CdSe prepared by precipitation from toluene and subsequently dissolved in DMF (a polar aprotic solvent), while Yan, Zhang and coworkers[29] described chiral CdSe prepared in $CHCl_3$ (non-polar aprotic solvent). Herein, we report the first comprehensive study of the effect of the 2nd stereogenic center as well as the effect of the type and distance of the functional group from the QD surface on the induced optical (UV-vis and emission) and chiroptical (induced CD shape and anisotropy) characteristics of CdS QDs using 17 structurally diverse chiral carboxylic acids. This work also describes the importance of the solvent during ligand exchange on the induced circular dichroism.

2. Experimental section

General Procedure for Phase Transfer Ligand Exchange Synthesis of Chiral QDs

A chiral carboxylic acid and TMAH were dissolved in methanol and cyclohexane was added. The mixture was then deoxygenated under vigorous stirring using three vacuum-N_2 cycles. A cyclohexane solution of oleic acid capped CdS QDs was added *via* a syringe to the deoxygenated mixture. The resulting reaction mixture was vigorously stirred at RT under N_2 in the absence of light for 30 min. The reaction mixture was then left to stand for 30 min to allow the phases to fully separate after which the MeOH layer was removed with a syringe, and the QDs functionalized with chiral acids were fully characterized.

The Fitting of the Absorption and CD Spectra

The fitting was done using Matlab (MathWorks, Inc. Mattick, MA). Each set of absorption and CD spectra was modeled as a linear combination of nine Gaussian profiles and first derivative Gaussian profiles, respectively. The number of Gaussian functions (nine) was determined from initial testing to be the minimum number to ensure a satisfactory fit to the data over the studied spectral range. Both UV-vis and CD spectra were fit simultaneously by minimizing the sum of squares between the experimental and the model spectra using the simplex algorithm as implemented in Matlab with the positions and widths of the individual Gaussian bands as adjustable parameters. The intensities of the individual bands within the UV-vis and CD spectra were obtained by a linear least squares fit at each step of the optimization routine. The fitting of each data set was performed several times with varying initial parameters to ensure the proper convergence of the fitted parameters.

Nuclear Magnetic Resonance (NMR) Spectroscopy

Solid state NMR. Magic angle spinning solid state NMR (MAS ssNMR) experiments were carried out on a Bruker Avance NEO 700 MHz NMR spectrometer equipped with a 4 mm E^{free} triple resonance HCN probe. Samples were packed into 4 mm Bruker MAS rotors. One dimensional (1D) ^{13}C ssNMR spectra were acquired using ^{1}H-^{13}C cross-polarization (CP) and ^{1}H decoupling during acquisition. ^{1}H-^{13}C CP was achieved with a 50-100% ramped 56 kHz ^{1}H and 45 kHz ^{13}C pulses for 1.0 ms. Spectra were acquired for 25 ms with 67 kHz of two-pulse phase modulated (TPPM) ^{1}H decoupling and with 4 s recycle delay. Experiments were performed at 258 K (variable temperature set point) and 10.0 kHz MAS frequency. All spectra were externally referenced to DSS using the adamantane downfield ^{13}C peak at 40.48 ppm.[30] Data were processed with TopSpin using cosine squared window function. **Solution NMR.** Solution NMR spectra were collected on a Bruker Avance NEO 700 MHz NMR spectrometer equipped with a solution 5-mm triple resonance inverse TCI CryoProbe and using a standard Bruker pulse sequence with a 30° flip angle ^{1}H pulse. The recycle delay was 1.0 s.

3. Results and discussion

3.1 Synthesis, optical and structural properties of MeOH-soluble QDs

As our previously reported QDs capped with carboxylic acid aggregated in water, and the majority of carboxylic acids did not induce chirality,[21] here we have explored a phase transfer into a less polar solvent. We have tested various water-free organic→organic phase transfer ligand exchange conditions using two immiscible organic solvents and found the cyclohexane-MeOH heterogenous mixture as the most suitable as judged by yields, stability, and chirality of CdS QDs. Even though MeOH is significantly less polar than water (relative permittivity ε_r = 33 *vs*. 78), it is still immiscible with hydrocarbons with the cyclohexane having lower solubility in MeOH than its acyclic counterpart hexane.[31, 32] Using ^{1}H NMR, we estimated the concentration of cyclohexane in MeOH to be ≈ 230 mg/mL (Figure S5). Oleic acid functionalized CdS QDs (OA-CdS) in cyclohexane with an average diameter of ⌀ = 4.1 nm (λ_{max} = 419.4 nm, E_g = 2.956 eV, Figure S1) as determined using Peng's equation[33] and an average hydrodynamic diameter of 6.5 nm as determined by DLS (Figure S2), have been used as a starting material for the cyclohexane→MeOH phase-transfer ligand exchange. All 17 chiral carboxylic acids selected for this study (Chart S1) successfully underwent ligand exchange within 30 min using an excess of the chiral acid and TMAH (see Table S1 for experimental conditions). The ligand exchange yields were >90% determined by UV-vis absorption spectroscopy

apart from the aliphatic and highly hydrophobic amino acids leucine and allo-leucine[34] which gave 40-50% yield. ^{1}H NMR data showed nearly quantitative replacement of oleic acid capping ligand by chiral carboxylic acid ligands, as judged by the integration of the signals corresponding to alkenyl protons of the oleic acids and Hα/Hβ hydrogens of the chiral acids (Figures S3-4). Attenuated total reflectance infrared (ATR-IR) data supported the loss of the native OA and confirmed full deprotonation of the carboxyl functional group of the carboxylic acid capping ligands. However, only small differences have been detected in the ATR-IR spectra of carboxylic acid-TMAH mixtures before and after the functionalization with CdS (Figures S7-S14).[35] Importantly, regardless of the structure of the chiral acid (*i.e.*, aliphatic, polar, acidic, basic and cyclic amino acids or methyl-, amino- or hydroxy-substituted mono- or dicarboxylic acids), the cyclohexane→MeOH phase transfer ligand exchange yielded stable MeOH-soluble carboxylic acid functionalized CdS QDs that did not show aggregation, and no precipitation has been observed after 10 min of centrifugation at 14,000×g. Of great importance is that no purification of chiral CdS QDs was required, and all chiral CdS QDs were used as prepared in MeOH solutions. Brightfield TEM and darkfield HAADF measurements were performed to characterize the chiral CdS QDs. TEM images of the L-Asp-CdS QDs (Figure 1a-c) and L-allo-Thr-CdS (Figure 1d-f) prepared by cyclohexane→ MeOH phase transfer ligand exchange showed (i) clear lattice fringes throughout the dots with a *d*-spacing of 3.34 Å corresponding to the (111) lattice plane of the CdS cubic (zinc blende) crystal structure and (ii) absence of chiral assemblies of QDs. UV-vis absorption spectra of chiral carboxylic acid capped CdS QDs showed that 12 chiral ligands caused a small (≤ 1.4 nm) red or blue shift of the lowest energy excitonic peak (λ_{max}; Figures 2a and S15-S31). On the other hand, His and allo-Thr induced a red shift of ~2.0-2.5 nm in the λ_{max} of CdS, while functionalization with allo-Thr, IsoSer, MA, and TA (all four having a hydroxy group on the Cα carbon and two additional coordinating functional groups) caused significant red shifts of 2.4, 5.6, 8.2, and 8.7 nm, respectively, corresponding to the optical band gap shifts to lower energy by approximately 17, 38, 56, and 60 meV. Ligand induced shift of the lowest energy excitonic peak relative to the initial sample has been previously reported for QDs as well as for magic-size clusters.[36-38] Weiss and collaborators proposed that the bathochromic shift was observed for the QDs with weakly bound ligands under fast or intermediate exchange (carboxylates are weakly bound to the surface of CdS) and originated from interactions of anions (such as hydroxide) with the surface of QDs.[37, 38]

Figure 1. Brightfield TEM images, darkfield HAADF images, and the grey scale cross-sections of (a-c) L-Asp-CdS and (d-f) L-allo-Thr-CdS (ØCdS = 4.2 nm). Insets in (a) and (e): Images of QDs showing lattice fringes corresponding to CdS (100) crystal planes with spacing of ~3.37 Å (box size: ~5 × 5 nm).

However, in our case, no simple correlation could be determined between the amount of TMAH used (the source of hydroxide anions in solution) and the observed shift of absorption maximum. This can be illustrated for instance comparing MA-CdS/Glu-CdS pair or Ser-CdS/IsoSer-CdS pair that displayed very different absorption maxima (427.6 *vs*. 420.8 nm for the former and 420.4 *vs*. 425.0 nm for the latter pair) despite each pair being prepared using identical amount of TMAH (Table S1). We hypothesized that the tridentate binding with carboxylate as the anchoring groups induced orbital hybridization of the HOMO of the capping ligand and the valence band of CdS that led to the decrease of the energy band gap and the subsequent red shift of the lowest energy excitonic band. The data indicated that the structure and the binding mode of chiral acids contributed to the observed optical bandgap highlighting the importance of optimizing the binding geometry of chiral capping ligands used in future optical and chiroptical applications.

Figure 2. (a) Wavelength of the chiral CdS lowest energy excitonic peak as a function of the chiral carboxylic acid capping ligand in methanol (x-axis bottom) and the shift of the wavelength of the chiral CdS lowest energy excitonic peak relative to the OA-CdS in cyclohexane ($\Delta\lambda_{max}$ in nm, x-axis top). (b) UV-vis absorption and (c) normalized emission spectra (λ_{exc} = 355 nm) of OA-CdS, L-MA-CdS and L-Ala-CdS QDs in MeOH. (d) Band-edge (λ_{em} = 434 and 437.5 nm) and trap-state (λ_{em} = 612.5 and 591 nm) photoluminescence decays and their two-exponential fits for L-Thr-CdS and L-MA-CdS in MeOH.

3.2. Fluorescence Properties of chiral QDs

Steady state and time-resolved fluorescence measurements were performed to characterize the effect of the capping ligands on the emission of chiral CdS QDs. Fluorescence spectra showed that the phase transfer ligand exchange of OA for chiral carboxylic acid ligands caused a decrease of the fluorescence quantum yields as well as a strong surface-defect state emission as has been previously observed for a toluene-water phase transfer system.[21] Fluorescence spectrum of OA-CdS QDs displayed a sharp peak at 431 nm (λ_{exc} = 355 nm) and a weak shoulder centered at 595 nm corresponding to the near band-edge emission and deep-trap emission, respectively (Figures 2c and S1). On the other hand, the fluorescence spectra of 15 out of 17 chiral carboxylic acid capped CdS QDs displayed intense deep trap emission centered at 610 nm and only weak exitonic band at ~436 nm (λ_{exc} = 355 nm, Figures 2c and S15-S32). The two notable exceptions were MA-CdS and TA-CdS QDs where the band-edge emission ≈450 nm was the dominant form of radiative decay (Figures 2c, S26 and S28). To better understand the impact of chiral coordinating ligands on emission of the CdS QDs, the fluorescence quantum yields and fluorescence lifetimes of band-edge and trap state emission of L-MA-CdS and L-Thr-CdS have been measured. L-MA-CdS displayed higher emission quantum yield (Φ) than L-Thr-CdS (3.3% *vs*. 1.8%) indicating that in L-MA-CdS the nonradiative recombination pathways have been eliminated better than in L-Thr-CdS QDs. Moreover, the integration of the intensity of the band-edge and trap-state emissions revealed that the band-edge emission was the major radiative relaxation pathway for L-MA-CdS being responsible for 64% of the total fluorescence quantum yield while the remaining 36% were assigned to the trap-state emission. On the other hand, band-edge emission accounted only for 17% of emitted light in L-Thr-CdS and the trap-state emission with 83% was the dominant radiative pathway. It is

apparent that L-MA coordination to the vacant sites of the surface Cd atoms also minimized the surface defects thus suppressing the nonradiative decay pathways. To gain further insight into the nature of emissive excited states, nanosecond time-resolved measurements have been performed on L-Thr-CdS and L-MA-CdS and the transient photoluminescence decays have been recorded (Figure 2d). Even though the band-edge and trap-state decay profiles were fitted to biexponential models, the actual decays were expected to be a broad distribution of states and were therefore more accurately represented by intensity-weighted average lifetimes (Table 1).[39] The L-MA-CdS displayed longer average lifetime for band-edge emission but shorter for trap-state emission than the L-Thr-CdS, supporting the fluorescence steady state data and quantum yield measurements. However, the average band-edge lifetimes of L-Thr-CdS and L-MA-CdS (2.9 and 10.0 ns) were much longer than those reported for direct band-edge recombination of an exciton.[40] They must have therefore originated in the shallow trap states located close to the band edge (*i.e.,* near band-edge states).[41]

Table 1. Fitted results of band-edge and trap states photoluminescence decays and emission quantum yields (Φ) of L-Thr-CdS and L-MA-CdS QDs.

	λ_{em} (nm)	τ1 (ns)	Rel (%)	τ2 (ns)	Rel (%)	τ_{mean} (ns)	Φ (%)
L-Thr-CdS	434	0.56	53.6	6.39	46.4	2.9	0.3
	612.5	1.80	4.2	36.1	95.8	35.4	1.5
L-MA-CdS	437.5	1.29	18	12.02	82	10.0	2.1
	591	1.29	7.2	22.19	92.8	19.7	1.2

The broad emission of L-Thr-CdS and L-MA-CdS centered around 600 nm decayed with a significantly longer average lifetimes (35.4 and 19.7 ns) than the band-edge emission. It has previously been reported that the formation of the deep-trap states responsible for the surface trap state emission of CdS occurred in ≥30 ps from shallow traps near the band gap states.[41] Hence, the slower decay observed in the 600 nm region originated from the emission from the deep trap-states. Importantly, similar lifetimes have been reported previously for deep-trap emission of CdS.[42, 43] Structural comparison revealed that, unlike majority of capping ligands used in this study, MA and TA lacked the amino group, had a hydroxy group on the Cα and a secondary carboxyl group. Our previous DFT studies revealed that tridentate binding is energetically favored for alpha-hydroxy-dicarboxylic acids on CdSe QDs.[21] Since (i) MSA lacked the amino group, had a methyl on the Cα and had a secondary carboxyl group, and (ii) LA lacked the amino group and had a hydroxy group on the Cα yet they both exhibited mostly deep-trap emission, it appears that the presence of Cα hydroxy group together with second carboxylic group are necessary for effective surface passivation as well as suppression of the nonradiative decay pathways.

3.3. Chiroptical Properties of QDs

A definite proof of successful phase transfer ligand exchange functionalization of CdS QDs with chiral carboxylic acid came from CD spectroscopy. OA-CdS QDs used as starting material in the ligand exchange which capped with achiral oleic acids were optically inactive and did not show any CD response. On the other hand, upon ligand exchange, all 17 chiral carboxylic acid ligands successfully induced chiroptical activity in CdS as evidenced by the CD signal in the 300-450 nm region of the electromagnetic spectrum, far away from the CD signal of the carboxylic acid capping ligands (<280 nm).[44-46] The presence of the CD signal confirmed binding of the chiral ligand to the surface of CdS and orbital hybridization with CdS. As expected, enantiomeric carboxylic acids induced mirror-image CD spectra in CdS QDs (Figures 3, 5 and 8). Since TEM did not show formation of chiral assemblies of QDs, the observed differences in induced circular dichroism originated from the different surface binding geometries of the chiral capping ligands.

In order to evaluate the influence of the ligand's structure on the chirality of CdS QDs, we have first utilized the CD and UV-vis absorption spectra to determine the anisotropic dissymmetry *g* factor (Table 2).[47, 48] Carboxylic acid ligands are bound to the surface of QDs *via* the carboxylate group (*i.e.*, C1 carbon) as the primary anchor point (the exception being cysteine which is attached to the QDs *via* sulfhydryl group).[49-52] Solution and solid state NMR data of cysteine capped CdSe supported multidentate binding *via* hydroxy or amino functional groups as secondary anchors.[3, 20, 27, 53-55] Computational studies on carboxylate ligand capped CdSe nanocrystals suggested multidentate binding to the surface of QDs with hydroxy groups providing secondary and tertiary anchor point.[21] As can be seen from Table 2, ligand structure had a pronounced effect on the chirality of CdS. However, comparison of the emission data with the CD anisotropy *g* factors showed no apparent correlation between effective surface passivation and/or suppression of the nonradiative decays and ligand induced anisotropy of QDs.

Table 2. CD anisotropy *g* factors of CdS QDs functionalized with chiral carboxylic acid ligands in MeOH.

Ligand	g_{λ}×10^{-4} (λ_{exband}, nm) [a]	g_{max}, ×10^{-4} (λ, nm) [b]
L-Ala	+0.01 (418.8)	-2.2 (396.5)
L-Asp	+0.21 (419.0)	-1.9 (386.0)
L-Cys	+0.35 (417.8)	+1.8 (425.0)
L-Glu	-0.64 (420.8)	-1.3 (387.0)
L-His	+0.13 (422.0)	-0.47 (430.0)
L-Ile	-1.1 (419.6)	-2.0 (386.0)
L-allo-Ile	-0.79 (419.8)	-2.9 (388.0)
L-Val	-0.75 (419.4)	-2.4 (382.0)
L-LA	+0.38 (419.4)	-2.8 (427.5)
L-MA	-0.29 (427.6)	-0.56 (376.5)
L-MSA	+0.12 (419.4)	+3.1 (427.5)
L-Ser	+1.2 (420.4)	-3.0 (392.5)
L-IsoSer	+0.61 (425.0)	+2.0 (380.0)
L-Pro	+0.09 (417.8)	-1.6 (397.0)
L-TA	+1.4 (428.2)	-4.3 (437.0)
L-Thr	+0.77 (420.2)	-3.3 (391.0)
L-allo-Thr	+0.33 (421.8)	-3.0 (391.5)

[a] CD anisotropy at the lowest energy excitonic band (λ_{exband}), [b] CD anisotropy at a CD band maximum (λ).

Anisotropy factor at the lowest energy exitonic band (g at λ_{max}) for CdS capped with L-enantiomers varied between -1.1×10^{-4} (L-Ile) and +1.2×10^{-4} (L-Ser) for ligands with a single stereogenic center and between -0.29×10^{-4} (L-MA) and +1.4×10^{-4} (L-TA) for ligands with two stereogenic centers. L-Ala induced the smallest CD anisotropy in CdS at λ_{max} (g_λ = +0.01×10^{-4} at 418.8 nm), while L-TA induced the largest (g_λ = +1.4×10^{-4} at 428.2 nm), giving rise to a 140-fold difference. L-His induced the smallest CD anisotropy at a CD band maximum (g_{max} = -0.47×10^{-4} at 430.0 nm), whereas L-TA induced the largest (g_{max} = -4.3×10^{-4} at 437.0 nm), yielding a 9-fold difference. Interestingly, attachment of the chiral ligand *via* the tightly bound sulfhydryl (thiol) group (*i.e.*, cysteine) did not yield higher CD anisotropy than the weakly bound carboxylate ligands (Table 2 and Figure S32). However, the anisotropy factor only gives a limited assessment of the ligand structure on the induced CD of QDs. For a thorough evaluation, the shape of the induced CD spectra of QDs must be compared for various isomeric capping ligands. Only then, a more profound understanding of the ligand-nanocrystals interplay can be achieved, and the fundamental mechanism of the chirality induction in semiconductor QDs can be determined.

3.3.1. The effect of a second stereogenic center: CD of CdS capped with epimers

Large majority of the work on chiral QDs focused on coordinating ligands with single chirality center attached via sulfur. Only two articles reported the effect of the multiple stereocenters on the CD anisotropy (g_{max}), and contradicting differences have been observed. Whereas similar g_{max} values have been reported for water-soluble CdSe functionalized with MA (single stereocenter) and TA (two stereocenters),[21] the CdSe dissolved in DMF displayed a 2-fold larger g_{max} for the latter.[28] However, both these studies suffered from one significant shortcoming: the introduction of the second stereogenic center also introduced a new functional group to the molecules. To effectively determine the effect of the second stereocenter, one must evaluate chiral ligands with two stereocenters that differ in chirality of the second stereocenter (*i.e.,* epimers), against a chiral ligand with one stereocenter where all three ligands share nearly identical chemical structure. For that purpose, we functionalized CdS with (i) epimers threonine/allo-threonine and compared their data with CdS capped with serine, and (ii) epimers isoleucine/allo-isoleucine and compared their data with CdS capped with valine (Chart 1). Epimers tend to have very different physical, chemical, and chiroptical properties, and the ligand induced CD anisotropy of QDs depends on (i) QD-ligand electronic coupling and (ii) the ligand binding geometry and ligand surface packing. Consequently, the presence of the second stereogenic center can either have constructive interaction with the existing center and thus lead to an enhancement of the ligand-induced CD anisotropy of QDs ("match") or a destructive interaction yielding a decrease of the CD anisotropy of QDs ("mismatch").

2nd stereocenter with coordinating functional group: CD of CdS functionalized with threonine, allo-threonine, and serine. We explored the CD spectra of CdS induced by serine (2-amino-3-hydroxypropanoic acid with a single stereocenter) with CD spectra induced by epimeric α-amino acids threonine and allo-threonine (2-amino-3-hydroxybutanoic acids with two stereocenters).

Chart 1: Structures of L-enantiomers of threonine, allo-threonine, serine, isoleucine, allo-isoleucine, and valine.

Ser, Thr, and allo-Thr (Chart 1) have a neutral coordinating electron-withdrawing amino functional group (a medium size polar L-type ligand with one set of lone pairs and an A value of 1.6)[56] at the Cα stereogenic center and a coordinating hydroxy group (a small polar L-type ligand with two sets of lone pairs and A-value of 0.87) at the Cβ. Ser, Thr and allo-Thr share the absolute configuration at the Cα amino center, but while Cβ carbon of Ser is achiral, Thr and allo-Thr have opposite absolute configuration at the Cβ hydroxy-center. All three ligands are bound to the surface *via* the carboxylate group (*i.e.*, C1 carbon), therefore, the NH_2 group at the Cα chirality center was located closer to the CdS surface than the OH group at the Cβ carbon.

The UV-vis absorption spectra of CdS functionalized with Ser, Thr, and allo-Thr revealed no significant change to the UV-vis spectral profile of CdS in comparison to OA-CdS QDs (Figures 3c, S18-S19, S24). As can be seen from Table 2, the addition of the second stereogenic center had a weak impact on the CD anisotropy, and Ser, Thr, and allo-Thr induced similar maximum anisotropies g_{max} = -3.0×10^{-4} (391 nm), -3.3×10^{-4} (391.5 nm), and -3.0×10^{-4} (392.5 nm), respectively. On the other hand, comparison of CD spectra of L-Ser-CdS, L-Thr-CdS and L-allo-Thr-CdS revealed significant differences in the CD signals, especially within the first excitonic band (above 400 nm). CD spectrum of the L-Ser-CdS showed positive CD bands at 415 and 358 and negative CD bands at 395 and 330 nm (Figure 3b). Comparison of CD spectra of L-(2*S*)-Ser-CdS with L-(2*S*, 3*R*)-Thr-CdS revealed (i) the appearance of a new positive CD band at 430 nm, (ii) the increase of the positive 415 nm CD band, and (iii) the hypsochromic shift of the 358 nm positive CD band to 350 nm, while only small intensity change was observed for the 395 nm negative CD band (Figure 3b; black and red curve). On the other hand, comparison with L-(2*S*, 3*S*)-allo-Thr showed opposite trends, *i.e.*, increase of the positive 415 nm CD band, and bathochromic shift of the 358 nm positive CD band to 364 nm (Figure 3b; black and blue curve).

Figure 3. (a) CD spectra of L- and D-Trh-CdS. (b) CD and (c) UV-vis spectra of L-Thr-, L-allo-Thr-, and L-Ser-CdS; [CdS] ≈ 1.5 μM. (d) Simulated CD and UV-vis spectra of L-Thr-CdS. (e) CD intensity (415 nm) and (f) wavelength of the CD band (≈358 nm) of Ser-, Thr-, and allo-Thr-CdS. [CdS] ≈ 1.5 μM.

Further analysis of the effects of the 2nd stereocenter demonstrated the following trends: (i) presence of the (3R) stereocenter (L-Thr) caused an increase of the positive CD band at 415 nm (Figure 3e) and a blue shift of the 358 mm CD band (Figure 3f), while the presence of (3S) stereocenter (L-allo-Thr) caused the opposite effects, *i.e.*, decrease of the 415 CD band intensity and a red shift of the 358 mm CD band. The analysis of the CD data of CdS functionalized with Ser/Thr/allo-Thr

revealed that the introduction of the second stereogenic center does not simply translated into increase of the CD anisotropy of QDs. The effect of two stereocenters on the induced chirality of CdS can be compared to the 'match/mismatch' concept known in the asymmetric induction in organic synthesis or in the 'conglomerate-racemate' crystallization. Laterally enantio-separated and racemic lattices of chiral ligands as well as chiral ligand patterns have also been reported on metallic surfaces.[57-61]

To better understand the above observed differences, we explored the binding of threonine to the surface of CdS QDs using ^{13}C magic angle spinning solid state NMR spectra (^{13}C MAS ssNMR; Figures 4 and S6).[3, 20, 53, 55, 62] We have measured spectra of L-Thr-CdS QDs (L-Thr/TMAH molar ratio 1:2; Figure 4, red spectrum) prepared by precipitation from the MeOH layer from the ligand exchange reaction mixture and compared it with spectra of solid L-Thr, neat solid (control A; Figure 4, black spectrum) and L-Thr/TMAH (molar ratio 1:2 mixture) prepared by evaporation of the MeOH layer from a cyclohexane/MeOH mixture (control B; Figure 4, purple spectrum). Since the ^{13}C chemical shift of the amino acid's carbonyl group has been shown to be sensitive to the environment,[63, 64] we have analyzed this region in detail. While the ^{13}C MAS ssNMR spectrum of control samples A and B showed one and two carbonyl peaks, respectively, the ^{13}C MAS ssNMR spectrum of L-Thr-CdS QDs prepared by precipitation from the MeOH layer (L-Thr/TMAH molar ratio 1:2) revealed several new broad peaks. The presence of new ^{13}C signals in the carbonyl region of L-Thr-CdS QDs is a direct evidence of the binding of L-Thr to the CdS surface, whereas the presence of multiple ^{13}C signals in the carbonyl region supports several concurrent multidentate (*i.e.,* bidentate and tridentate) binding geometries and/or ionization states (Figure 4, red curve; new ^{13}C carbon peaks are shown in dashed boxes).

Figure 4. Carbonyl region of the ^{13}C MAS ssNMR spectra of L-Thr-CdS. Black dashed rectangles encompass new signals in L-Thr-CdS QDs. Spectra were referenced to DSS (sodium salt of 2,2-dimethyl-2-silapentane-5-sulphonic acid). The spectra were acquired utilizing cross polarization from ^{1}H to ^{13}C, the areas under the signals are not necessarily proportional to the number of carbons, and the amount of each form cannot be determined quantitatively.

To further enhance the understanding of differences in CD spectra of CdS capped with L-Ser, L-Thr and L-allo-Thr, we have reconstructed their CD spectra using linear sums of the derivatives of the Gaussian functions obtained by the fitting of the corresponding absorption spectra (see Methods and Figures 3d, S33-S35).[25] The derivative Gaussian functions obtained from the fit to the absorption spectrum, *i.e.*, those corresponding to the observable absorption peaks, were not sufficient to adequately model the CD. Rather, additional Gaussian functions were necessary to account for the CD features suggesting a non-conservative splitting of the bands of the electronic spectra. A comparison of the reconstructed CD spectra of L-(2*S*)-Ser-CdS with L-(2*S*, 3*R*)-Thr for the low energy band edge transitions showed that the introduction of the opposite '3*R*' chirality on Cβ led to (i) a significant increase of magnitude of the derivative line of the lowest energy band edge transition ($1S_{3/2}1S_e$,),[65] and (ii) an decrease of magnitude and decrease of the energy split ΔE_i of the derivative line of the 2nd band edge transition ($2S_{3/2}1S_e$) thus leading to the increase of the CD intensity within the exitonic region (*i.e.*, match effect). On the other hand, the introduction of the identical '3S' chirality using L-(2*S*, 3*S*)-allo-Thr had the exact opposite effect (*i.e.*, mismatch).

2nd stereocenter with non-coordinating functional group: CD of CdS functionalized with isoleucine, allo-isoleucine, and valine. Using valine (Val, 2-amino-3-methylbutanoic acid), an α-amino acid with a single stereocenter as a control, we evaluated the effect of the 2nd stereogenic center on CD characteristics in epimeric Ile and allo-Ile (2-amino-3-methylpentanoic acid), α-amino acids with two stereocenters. All three ligands are bound to the surface via the carboxylate group (i.e., C1 carbon) and have non-coordinating methyl groups at the Cβ carbon (a medium size non-polar group with A-value of 1.7): however, while Cβ carbon of Val is achiral, the Cβ of Ile and allo-Ile are chiral with opposite absolute configurations. The UV-vis absorption spectra of Val-CdS, Ile-CdS, and allo-Ile-CdS revealed nearly identical spectra in comparison to OA-CdS QDs (Figures 2a, 5c, S16-S17). The CD spectrum of L-Val-CdS lied in between the CD spectra of L-Ile-CdS and L-allo-Ile-CdS having positive CD bands at 410 and 360 and negative CD bands at 420, 380, and 345 nm (Figure 5b, black curve). CD spectrum of L-(2S, 3S)-Ile-CdS had decreased intensity of the 380 and 360 nm CD bands (Figure 5b; black and green curves) while the CD spectrum of the epimeric L-(2S, 3R)-allo-Ile-CdS displayed the exactly opposite trends, *i.e.*, increase of 380 and 360 nm CD bands (Figure 5b; black and magenta curves). In comparison with L-Val-CdS (g_λ = -0.75×10^{-4} at 419.4 nm, g_{max} = 2.4×10^{-4} at 382 nm), the L-Ile induced larger anisotropy at the lowest energy excitonic band g_λ but smaller g_{max} (-1.1×10^{-4} at 419.6 nm; -2.0×10^{-4} at 386 nm) while the L-allo-Ile had similar g_λ but larger g_{max} (-0.79×10^{-4} at 419.8 nm; -2.9×10^{-4} at 388 nm). From the CD data it is apparent the presence of the 2nd stereogenic center led to increase/decrease of the CD intensity in accordance with 'match/mismatch' concept. However, the changes caused by the non-coordinating methyl group stereocenter (allowing only for a bidentate binding of Ile/allo-Ile/Val) were less notable than the one caused by OH group stereocenter in Thr/allo-Thr/Ser-CdS.

Figure 5. (a) CD spectra of L- and D-Ile-CdS; [CdS] ≈ 0.7 μM. (b) CD and (c) UV-vis spectra of Ile-, allo-Ile-, and Val-CdS; [CdS] ≈ 0.7 μM.

In summary, the analysis of CD data of CdS functionalized with Thr, allo-Thr, Ser as well as with Ile, allo-Ile, and Val revealed that an increased number of stereogenic centers do not directly translate to a higher CD anisotropy. Rather, the configurational 'match/mismatch' originating from ligand's multidentate binding (*i.e.*, simultaneous interaction between CdS and chiral acids *via* carboxyl, amino and hydroxy groups) and ligand-ligand interaction on the surface of QDs must be taken under consideration.

3.3.2. The effect of position of functional groups within ligand: CdS capped with positional isomers

The position of functional groups within the chiral ligands as well as their distance from the surface of QDs are structural factors that affect the binding mode and would affect ligand-QDs electronic coupling. Yet these parameters have never been studied. These parameters can be explored using positional isomers of carboxylic acids bound to the surface *via* the carboxylate group. Positional isomers are constitutional isomers that have the same carbon skeleton and the same functional groups but different position of functional groups within the molecule. Amino acids serine (Ser) and isoserine (IsoSer) are positional isomers: serine has the amino group at the Cα stereogenic center near the carboxyl anchor group and hydroxy group at the achiral Cβ carbon, while isoserine has them flipped (Figure 6). UV-vis absorption spectra showed that the presence of the hydroxy group near the anchoring group (IsoSer) induced a 5.6 nm red shift of λ_{max} in comparison to OA-CdS while the amino group only caused a 1.0 nm red shift (Figures 2a, S24-S25).

Figure 6. (a) CD and (b) UV-vis absorption spectra of L-Ser-CdS and L-IsoSer-CdS; [CdS] ≈ 1.5 μM.

The CD spectrum of L-IsoSer-CdS displayed positive CD bands at 420, 380, and 325 nm and negative CD bands 400 and 365 nm (Figure 6a; orange curve). The comparison of the CD spectra of L-Ser-CdS and L-IsoSer-CdS showed significant differences in intensities and position of the CD bands (Figure 6a). The differences in the position of the CD bands above 370 nm can be explained by the change in the band gap as both ligands displayed a (+/-/+; from longer to shorter wavelength) CD pattern above 350 nm with the CD of IsoSer-CdS red-shifted by approximately 7 nm mirroring the λ_{max} shift. On the other hand, mirror-image signals have been observed for L-Ser-CdS and L-IsoSer-CdS below 375 nm. L-Ser induced larger CD anisotropy in the CdS (g_{max} = -3.0×10^{-4} at 392.5 nm) than L-IsoSer (g_{max} = -2.0×10^{-4} at 380.0 nm) revealing that the presence of amino group near the surface induced stronger anisotropy than hydroxy group. Overall, it is not the type of functional groups a capping ligand carry but rather their position within the ligand that defines the ligand's surface binding, ligand-QD electronic coupling and the induced CD of QDs.

3.3.3. The effect of a functional group structure: CdS capped with structural analogs

Structural analogs are ideally suited to evaluate the role of a functional group of a chiral ligand on the induced chirality of QDs as they share the same carbon chain (molecular skeleton) but differ in functional group(s) attached to it. Utilizing the analogs, we studied the effect of a single functional group variation of monocarboxylic and dicarboxylic acids on their UV-vis absorption and induced CD spectra.

Monocarboxylic acids. Monocarboxylic acids can only yield monodentate and bidentate binding geometry *via* the carboxyl group as the anchor group and with easily predictable distance between the surface and the functional group at the chiral center. By functionalizing CdS QDs with lactic acid (LA) and alanine (*i.e.*, monocarboxylic acid structural analogs), we explored the effect of amino group *vs.* hydroxy group at the Cα stereogenic center on CD in polar protic solvent MeOH (Figure 7). The Ala and LA ligands interacted with the CdS surface *via* the carboxylate group with a proposed bidentate binding through the coordinating amino or hydroxy moieties.

Figure 7. (a) CD and (b) UV-vis absorption spectra of L-Ala-CdS and L-LA-CdS; [CdS] ≈ 1.5 μM.

Comparison of the UV-vis absorption spectra of L-LA-CdS with L-Ala-CdS revealed similar effect of LA and Ala on the electronic properties of CdS with $\Delta\lambda_{max}$ shift of 0.6 nm (Figures 2a and 7b). Previous reports on the effect of the α-substituents on the CD of monocarboxylic acid capped QDs were conducted in chloroform (a non-polar aprotic solvent) and DMF (polar aprotic solvent) and reported that the functional groups affected the intensity of the CD signal but not the overall shape of the CD spectra.[29] Yet, the CD spectra of Ala-CdS and LA-CdS showed substantial differences in the position of the CD bands as well as their intensity. CD spectrum of L-LA-CdS had an intense (-/+) bisignate CD within the lowest energy excitonic band (428 and 414 nm, Figure 7a) with a maximum anisotropy g_{max} of -2.8×10^{-4} (427.5 nm). On the other hand, CD of the L-Ala-CdS showed weak blue-shifted (-/+) bisignate signal (425 and 412 nm) and a maximum anisotropy g_{max} of -2.2×10^{-4} (396.5 nm). Although a direct comparison with the previous reports was not possible, appearance of very different CD spectra for L-Ala-CdS and L-LA-CdS suggest that the presence of the polar protic solvent MeOH resulted in different electronic interactions between chiral ligands and the surface of QDs than the previously explored QDs in aprotic solvents. Altogether, the data underline the important role that the solvent plays in (1) the interplay between achiral QDs and chiral capping ligand and (2) observed induced CD spectrum of QDs.

Dicarboxylic acids. The role of the α-substituents of dicarboxylic acids on the CD of QDs has not been reported. Unlike their monocarboxylic counterparts, dicarboxylic acids can participate in bidentate as well as tridentate binding and can bind to the surface *via* either of the two or both carboxyl groups. Therefore, several possible binding geometries can exist rendering the surface binding more complex. To study the effect of one type of coordinating group (polar hydroxy group) and two types of non-coordinating groups (polar ammonium and nonpolar methyl group) on the UV- vis absorption and induced CD spectra of CdS we have selected three chiral α-substituted butanedioic acids: malic acid (Cα-hydroxy group), aspartic acid (Cα-ammonium group), and methylsuccinic acid (Cα-methyl group). UV-vis absorption spectrum of MA-CdS showed a red shifted first excitonic band ($\Delta\lambda_{max}$ = +8.2 nm) in comparison the OA-CdS, while only small shifts have been recorded for L-Asp-CdS ($\Delta\lambda_{max}$ = -0.4 nm) and L-MSA-CdS (no $\Delta\lambda_{max}$ change) (Figures 8b). Similar red shift was observed for L-IsoSer-CdS Figure 6b) but not for L-LA-CdS (Figure 7b), even though all these ligands had Cα hydroxy groups. It appeared that an α-OH group participating in a tridentate binding (L-IsoSer and L-MA) was responsible for the observed red shift of the λ_{max} since L-LA could only yield bidentate binding. Unlike in the previous

reports, the CD spectra of Asp-CdS, MA-CdS and MSA-CdS QDs showed significant differences not only in CD anisotropies (Table 2) but also in the CD profiles (Figure 8a). The observed CD differences were easily rationalized by different binding geometries originating from the α-substituents. Our TD-DFT geometry optimized cluster structures have shown L-Asp bound to the surface of QDs *via* the bidentate binding (two carboxylates), whereas the L-MA yielded a tridentate binding geometry (two carboxylates and the hydroxy group).[21] Interestingly, L-MSA-CdS and L-Aps-CdS displayed significantly larger g_{max} ($+3.1\times10^{-4}$ at 427.5 nm and -1.9×10^{-4} at 386.0 nm) than the L-MA-CdS (-0.56×10^{-4} at 376.5 nm) despite having only two coordinating groups (two carboxylates). These data suggested that the induced CD signal did not originate from the ligand-induced chiral distortion of the most outer layers of QDs (where a stereoselective tridentate binding of MA was expected to be more efficient) but rather from the ligand-QD orbital hybridization.

Figure 8. (a) CD and (b) UV-vis absorption spectra of L-Asp-CdS (blue curve), L-MA-CdS (red curve), and L-MSA-CdS (black curve) prepared by cyclohexane→MeOH ligand exchange; [CdS] ≈ 1.5 μM. (c) CD spectra of L-MA-CdS (red curve) and L-TA-CdS (green curve) prepared by cyclohexane→MeOH ligand exchange. (d) CD spectra of L-MA-CdS prepared by (i) cyclohexane→MeOH ligand exchange (red solid curve) and (ii) precipitated from toluene, then redissolved in MeOH (red dotted curve).

Another intriguing observation came by comparing CD spectra of L-(*2S*)-MA-CdS and L-(*2R*,*3R*)-TA-CdS, a dicarboxylic acid that contained one additional stereogenic center at Cβ with a hydroxy group. We and others have previously shown that L-MA-CdSe and L-TA-CdSe gave rise to mirror-image CD spectra, regardless whether they were prepared by toluene→water ligand exchange[21] or precipitated from toluene and resuspended in organic solvent.[28] However, when we prepared L-MA-CdS and L-TA-CdS by cyclohexane→MeOH ligand exchange, we did not observe mirror-image CD spectra. (Figure 8c). To eliminate the possibility that the observed CD differences originated from the use of CdS, we have prepared L-MA-CdS and L-TA-CdS (i) by toluene→water ligand exchange as well as (ii) by precipitation from toluene followed by resuspension in MeOH, and again, we observed mirror-image CD spectra (Figure S36). Motivated by these observations, we have proceeded to test the effect of the two very different ligand exchange procedures on the CD characteristics of L-MA functionalized CdS in MeOH. As can be seen in the Figure 8d, (i) L-MA-CdS prepared by cyclohexane→MeOH ligand exchange and (ii) L-MA-CdS prepared by precipitation from toluene followed by resuspension in MeOH displayed strikingly different CD spectra (shape and intensity), revealing that the induced chirality of CdS depended not only on the capping ligand or solvent but, as importantly, on the ligand exchange procedure. Our data underline that different surface binding geometries and different chiroptical properties can be obtained by simply modifying the ligand exchange thus providing alternative means to tune the induced CD of QDs. Further studies will be needed to fully comprehend the role of individual chemical components and experimental parameters.

4. Conclusions

We reported the first synthesis of non-aggregating chiral QDs with high chiroptical quality that did not require any purification and displayed strong, well-resolved, and time-stable CD signal. Absorption and emission studies revealed that the carboxylate capping ligands can tune the band gap by up to 65 meV as well as control the band gap and deep trap emission pathways. The presence of Cα hydroxy group together with second carboxylic group were necessary for effective QDs surface passivation as well as suppression of the nonradiative decay pathways resulting in a strong band edge emission. Contrary to previous reports, our comprehensive study revealed that the addition of a 2nd stereogenic center did not automatically lead to an increase of the CD anisotropy of QDs, but rather match/mismatch cooperativity effects must be considered in the transfer of the chirality from the capping ligands to the achiral nanocrystals. Variation in position of functional group as well as the chiral identity of the functional groups impacted both the shape and anisotropy of the induced CD spectra and revealed the importance of functional groups coordination and polarity on the binding geometry and induced chiroptical properties. Finally, we have described the first example where CD spectra of QDs capped with the same ligand and dissolved in the same solvent, displayed very different spectral profiles (both CD shape and CD anisotropy) emphasizing the importance of the ligand exchange protocol on the ligand's binding mode. Determination of the structural factors that control induced CD will help better understand the role that the ligands' structure plays in the structural, optical and chiroptical properties of chiral QDs. We anticipate that the results will open new avenues for the development and rational design of not only optically active QDs but also other areas of colloidal QDs applications, including spintronics, CPL emitters and luminescent probes and labels, which all rely on ligand-matter interface.

Author contributions

Y. A. J.: investigation, validation, formal analysis, and writing; Y. H. K.: investigation, validation, formal analysis, and writing; S. H.: investigation and validation; B. M. L.: investigation and formal analysis; J. K.: investigation, formal analysis, and methodology; K. V.: conceptualization, funding acquisition, investigation, resources, supervision, writing, and project administration; M. B.: conceptualization, investigation, writing, supervision, and project administration.

Conflicts of interest

There are no conflicts to declare.

Acknowledgements

This work was supported in part by the National Science Foundation (award CBET 1403947; KV), Yonsei University (MB) and the University of New Hampshire (KV, YHK, YAJ). The 700

MHz NMR was purchased by NSF MRI funds (award DBI 1828319; KV) with additional support from the UNH Center for Integrated Biomedical and Bioengineering Research (CIBBR), established through a grant from the National Institute of General Medical Sciences (NIGMS) of the National Institutes of Health (award P20GM113131). We thank Dr. C.A. Caputo and C. Wilson (UNH) for their assistance with time resolved fluorescence. YHK thanks the Summer Teaching Assistant Fellowship from the University of New Hampshire.

References

1. Moloney, M. P.; Gun'ko, Y. K.; Kelly, J. M., Chiral Highly Luminescent CdS Quantum Dots. *Chem. Commun. (Cambridge, U. K.)* **2007,** (38), 3900-3902.
2. Elliott, S. D.; Moloney, M. P.; Gun'ko, Y. K., Chiral shells and achiral cores in CdS quantum dots. *Nano Lett.* **2008,** *8* (8), 2452-2457.
3. Tohgha, U.; Varga, K.; Balaz, M., Achiral CdSe quantum dots exhibit optical activity in the visible region upon post-synthetic ligand exchange with d- or l-cysteine. *Chem. Commun. (Cambridge, U. K.)* **2013,** *49* (18), 1844-1846.
4. Tohgha, U.; Deol, K. K.; Porter, A. G.; Bartko, S. G.; Choi, J. K.; Leonard, B. M.; Varga, K.; Kubelka, J.; Muller, G.; Balaz, M., Ligand induced circular dichroism and circularly polarized luminescence in CdSe quantum dots. *ACS Nano* **2013,** *7* (12), 11094-11102.
5. Gao, X.; Zhang, X.; Deng, K.; Han, B.; Zhao, L.; Wu, M.; Shi, L.; Lv, J.; Tang, Z., Excitonic Circular Dichroism of Chiral Quantum Rods. *J. Am. Chem. Soc.* **2017,** *139* (25), 8734-8739.
6. Cheng, J. J.; Hao, J. J.; Liu, H. C.; Li, J. G.; Li, J. Z.; Zhu, X.; Lin, X. D.; Wang, K.; He, T. C., Optically Active CdSe-Dot/CdS-Rod Nanocrystals with Induced Chirality and Circularly Polarized Luminescence. *ACS Nano* **2018,** *12* (6), 5341-5350.
7. Shao, X.; Zhang, T.; Li, B.; Zhou, M.; Ma, X.; Wang, J.; Jiang, S., Chiroptical Activity of Type II Core/Shell Cu2S/CdSe Nanocrystals. *Inorg. Chem.* **2019,** *58* (9), 6534-6543.
8. Gao, X.; Zhang, X.; Zhao, L.; Huang, P.; Han, B.; Lv, J.; Qiu, X.; Wei, S.-H.; Tang, Z., Distinct Excitonic Circular Dichroism between Wurtzite and Zincblende CdSe Nanoplatelets. *Nano Lett.* **2018,** *18* (11), 6665-6671.
9. Sun, M.; Xu, L.; Qu, A.; Zhao, P.; Hao, T.; Ma, W.; Hao, C.; Wen, X.; Colombari, F. M.; de Moura, A. F.; Kotov, N. A.; Xu, C.; Kuang, H., Site-selective photoinduced cleavage and profiling of DNA by chiral semiconductor nanoparticles. *Nature Chem.* **2018,** *10* (8), 821-830.
10. Wawrzyńczyk, D.; Szeremeta, J.; Samoć, M.; Nyk, M., Size-dependent emission kinetics and sensing capabilities of CdSe quantum dots functionalized with penicillamine ligands. *Sens. Actuators B Chem.* **2017,** *252*, 483-491.
11. Martynenko, I. V.; Kuznetsova, V. A.; Litvinov, I. K.; Orlova, A. O.; Maslov, V. G.; Fedorov, A. V.; Dubavik, A.; Purcell-Milton, F.; Gun'ko, Y. K.; Baranov, A. V., Enantioselective cellular uptake of chiral semiconductor nanocrystalsd. *Nanotechnology* **2016,** *27* (7), 075102.
12. Kuznetsova, V. A.; Visheratina, A. K.; Ryan, A.; Martynenko, I. V.; Loudon, A.; Maguire, C. M.; Purcell-Milton, F.; Orlova, A. O.; Baranov, A. V.; Fedorov, A. V.; Prina-Mello, A.; Volkov, Y.; Gun'Ko, Y. K., Enantioselective cytotoxicity of ZnS:Mn quantum dots in A549 cells. *Chirality* **2017,** *29* (8), 403-408.
13. Wang, X.; Hao, J.; Cheng, J.; Li, J.; Miao, J.; Li, R.; Li, Y.; Li, J.; Liu, Y.; Zhu, X.; Liu, Y.; Sun, X. W.; Tang, Z.; Delville, M.-H.; He, T.; Chen, R., Chiral CdSe nanoplatelets as an ultrasensitive probe for lead ion sensing. *Nanoscale* **2019,** *11* (19), 9327-9334.
14. Yeom, J.; Yeom, B.; Chan, H.; Smith, K. W.; Dominguez-Medina, S.; Bahng, Joong H.; Zhao, G.; Chang, W.-S.; Chang, S.-J.; Chuvilin, A.; Melnikau, D.; Rogach, A. L.; Zhang, P.; Link, S.; Král, P.; Kotov, N. A., Chiral templating of self-assembling nanostructures by circularly polarized light. *Nat. Mater.* **2015,** *14* (1), 66-72.
15. Bloom, B. P.; Kiran, V.; Varade, V.; Naaman, R.; Waldeck, D. H., Spin Selective Charge Transport through Cysteine Capped CdSe Quantum Dots. *Nano Lett.* **2016,** *16* (7), 4583-4589.
16. Bloom, B. P.; Graff, B. M.; Ghosh, S.; Beratan, D. N.; Waldeck, D. H., Chirality Control of Electron Transfer in Quantum Dot Assemblies. *J. Am. Chem. Soc.* **2017,** *139* (26), 9038-9043.
17. Gao, X.; Han, B.; Yang, X.; Tang, Z., Perspective of Chiral Colloidal Semiconductor Nanocrystals: Opportunity and Challenge. *J. Am. Chem. Soc.* **2019,** *141* (35), 13700-13707.
18. Kuznetsova, V.; Gromova, Y.; Martinez-Carmona, M.; Purcell-Milton, F.; Ushakova, E.; Cherevkov, S.; Maslov, V.; Gun'ko, Y. K., Ligand-induced chirality and optical activity in semiconductor nanocrystals: theory and applications. *Nanophotonics* **2021,** *10* (2), 797-824.
19. Kwon, Y. H.; Tannir, S.; Balaz, M.; Varga, K., Apple juice and red wine induced mirror-image circular dichroism in quantum dots. *Chirality* **2021**, htpps://doi.org/10.1002/chir.23380.
20. Choi, J. K.; Haynie, B. E.; Tohgha, U.; Pap, L.; Elliott, K. W.; Leonard, B. M.; Dzyuba, S. V.; Varga, K.; Kubelka, J.; Balaz, M., Chirality Inversion of CdSe and CdS Quantum Dots Without Changing the Stereochemistry of Capping Ligand. *ACS Nano* **2016,** *10* (3), 3809-3815.
21. Varga, K.; Tannir, S.; Haynie, B. E.; Leonard, B. M.; Dzyuba, S. V.; Kubelka, J.; Balaz, M., CdSe Quantum Dots Functionalized with Chiral, Thiol-Free Carboxylic Acids: Unraveling Structural Requirements for Ligand-Induced Chirality. *ACS Nano* **2017,** *11* (10), 9846-9853.
22. Suzuki, N.; Wang, Y. C.; Elvati, P.; Qu, Z. B.; Kim, K.; Jiang, S.; Baumeister, E.; Lee, J.; Yeom, B.; Bahng, J. H.; Lee, J.; Violi, A.; Kotov, N. A., Chiral Graphene Quantum Dots. *ACS Nano* **2016,** *10* (2), 1744-1755.
23. Kuno, J.; Imamura, Y.; Katouda, M.; Tashiro, M.; Kawai, T.; Nakashima, T., Inversion of Optical Activity in the Synthesis of Mercury Sulfide Nanoparticles: Role of Ligand Coordination. *Angew. Chem., Int. Ed.* **2018,** *57* (37), 12022-12026.
24. Shao, X.; Wu, Y.; Jiang, S.; Li, B.; Zhang, T.; Yan, Y., Impact of native achiral ligands on the chirality of enantiopure cysteine stabilized CdSe nanocrystals. *J. Mater. Chem. C* **2021,** *9* (2), 555-561.
25. Ben-Moshe, A.; Teitelboim, A.; Oron, D.; Markovich, G., Probing the Interaction of Quantum Dots with Chiral Capping Molecules Using Circular Dichroism Spectroscopy. *Nano Lett.* **2016,** *16* (12), 7467-7473.
26. Purcell-Milton, F.; Visheratina, A. K.; Kuznetsova, V. A.; Ryan, A.; Orlova, A. O.; Gun'ko, Y. K., Impact of Shell Thickness on Photoluminescence and Optical Activity in Chiral CdSe/CdS Core/Shell Quantum Dots. *ACS Nano* **2017,** *11* (9), 9207-9214.
27. Kuznetsova, V. A.; Mates-Torres, E.; Prochukhan, N.; Marcastel, M.; Purcell-Milton, F.; O'Brien, J.; Visheratina, A. K.; Martinez-Carmona, M.; Gromova, Y.; Garcia-Melchor, M.; Gun'ko, Y. K., Effect of Chiral Ligand Concentration and Binding Mode on

Chiroptical Activity of CdSe/CdS Quantum Dots. *ACS Nano* **2019,** *13* (11), 13560-13572.
28. Puri, M.; Ferry, V. E., Circular Dichroism of CdSe Nanocrystals Bound by Chiral Carboxylic Acids. *ACS Nano* **2017,** *11* (12), 12240-12246.
29. Wu, Y.; Shao, X.; Zhou, Y.; Jiang, S.; Zhang, T. Y.; Yan, Y., Effect of alpha-substitute group on the chirality of monocarboxylic acid stabilized CdSe nanocrystals. *Nanotechnology* **2021,** *32* (37).
30. Morcombe, C. R.; Zilm, K. W., Chemical shift referencing in MAS solid state NMR. *J. Magn. Reson.* **2003,** *162* (2), 479-486.
31. Trejo, A.; Yañez, P.; Eustaquio-Rincón, R., Liquid−Liquid Coexistence Curves for Binary Systems: Methanol + Cyclohexane and + Several Isomers of Hexane. *J. Chem. Eng. Data* **2006,** *51* (3), 1070-1075.
32. Kiser, R. W.; Johnson, G. D.; Shetlar, M. D., Solubilities of Various Hydrocarbons in Methanol. *J. Chem. Eng. Data* **1961,** *6* (3), 338-341.
33. Yu, W. W.; Qu, L.; Guo, W.; Peng, X., Experimental Determination of the Extinction Coefficient of CdTe, CdSe, and CdS Nanocrystals. *Chem. Mater.* **2003,** *15* (14), 2854-2860.
34. Monera, O. D.; Sereda, T. J.; Zhou, N. E.; Kay, C. M.; Hodges, R. S., Relationship of sidechain hydrophobicity and α-helical propensity on the stability of the single-stranded amphipathic α-helix. *J. Pept. Sci.* **1995,** *1* (5), 319-329.
35. Hay, M. B.; Myneni, S. C. B., Structural environments of carboxyl groups in natural organic molecules from terrestrial systems. Part 1: Infrared spectroscopy. *Geochim. Cosmochim. Acta* **2007,** *71* (14), 3518-3532.
36. Nevers, D. R.; Williamson, C. B.; Hanrath, T.; Robinson, R. D., Surface chemistry of cadmium sulfide magic-sized clusters: a window into ligand-nanoparticle interactions. *Chem. Commun. (Cambridge, U. K.)* **2017,** *53* (19), 2866-2869.
37. Arcudi, F.; Westmoreland, D. E.; Weiss, E. A., Colloidally Stable CdS Quantum Dots in Water with Electrostatically Stabilized Weak-Binding, Sulfur-Free Ligands. *Chem. Eur. J.* **2019,** *25* (63), 14469-14474.
38. Thompson, C. M.; Kodaimati, M.; Westmoreland, D.; Calzada, R.; Weiss, E. A., Electrostatic Control of Excitonic Energies and Dynamics in a CdS Quantum Dot through Reversible Protonation of Its Ligands. *J. Phys. Chem. Lett.* **2016,** *7* (19), 3954-3960.
39. Fišerová, E.; Kubala, M., Mean fluorescence lifetime and its error. *J. Lumin.* **2012,** *132* (8), 2059-2064.
40. Misawa, K.; Yao, H.; Hayashi, T.; Kobayashi, T., Superradiance quenching by confined acoustic phonons in chemically prepared CdS microcrystallites. *J. Chem. Phys.* **1991,** *94* (6), 4131-4140.
41. O'Neil, M.; Marohn, J.; McLendon, G., Picosecond measurements of exciton trapping in semiconductor clusters. *Chem. Phys. Lett.* **1990,** *168* (2), 208-210.
42. Veamatahau, A.; Jiang, B.; Seifert, T.; Makuta, S.; Latham, K.; Kanehara, M.; Teranishi, T.; Tachibana, Y., Origin of surface trap states in CdS quantum dots: relationship between size dependent photoluminescence and sulfur vacancy trap states. *Phys. Chem. Chem. Phys.* **2015,** *17* (4), 2850-2858.
43. Wu, F.; Zhang, J. Z.; Kho, R.; Mehra, R. K., Radiative and nonradiative lifetimes of band edge states and deep trap states of CdS nanoparticles determined by time-correlated single photon counting. *Chem. Phys. Lett.* **2000,** *330* (3), 237-242.
44. Katzin, L. I.; Gulyas, E., Absorption, rotatory dispersion, and circular dichroism studies on some hydroxy and amino acids. *J. Am. Chem. Soc.* **1968,** *90* (2), 247-251.
45. Nishino, H.; Kosaka, A.; Hembury, G. A.; Matsushima, K.; Inoue, Y., The pH dependence of the anisotropy factors of essential amino acids. *J. Chem. Soc., Perkin Trans. 2* **2002,** (3), 582-590.
46. Amdursky, N.; Stevens, M. M., Circular Dichroism of Amino Acids: Following the Structural Formation of Phenylalanine. *ChemPhysChem* **2015,** *16* (13), 2768-2774.
47. Ben Moshe, A.; Szwarcman, D.; Markovich, G., Size dependence of chiroptical activity in colloidal quantum dots. *ACS Nano* **2011,** *5* (11), 9034-9043.
48. Ben-Moshe, A.; Maoz, B. M.; Govorov, A. O.; Markovich, G., Chirality and chiroptical effects in inorganic nanocrystal systems with plasmon and exciton resonances. *Chem. Soc. Rev.* **2013,** *42* (16), 7028-7041.
49. Fritzinger, B.; Capek, R. K.; Lambert, K.; Martins, J. C.; Hens, Z., Utilizing Self-Exchange To Address the Binding of Carboxylic Acid Ligands to CdSe Quantum Dots. *J. Am. Chem. Soc.* **2010,** *132* (29), 10195-10201.
50. Majetich, S. A.; Carter, A. C.; Belot, J.; McCullough, R. D., 1H NMR Characterization of the CdSe Nanocrystallite Surface. *J. Phys. Chem.* **1994,** *98* (51), 13705-13710.
51. Döllefeld, H.; Hoppe, K.; Kolny, J.; Schilling, K.; Weller, H.; Eychmüller, A., Investigations on the stability of thiol stabilized semiconductor nanoparticles. *Phys. Chem. Chem. Phys.* **2002,** *4* (19), 4747-4753.
52. Tamukong, P. K.; Peiris, W. D. N.; Kilina, S., Computational insights into CdSe quantum dots' interactions with acetate ligands. *Physical Chemistry Chemical Physics* **2016,** *18* (30), 20499-20510.
53. Kurihara, T.; Noda, Y.; Takegoshi, K., Capping Structure of Ligand–Cysteine on CdSe Magic-Sized Clusters. *ACS Omega* **2019,** *4* (2), 3476-3483.
54. Onoda, A.; Igarashi, M.; Naganawa, S.; Sasaki, K.; Ariyasu, S.; Yamamura, T., Circular Dichroism of Neutral Zinc Porphyrin-Oligonucleotide Conjugates Modified with Flexible Linker. *Bull. Chem. Soc. Jpn.* **2009,** *82* (10), 1280-1286.
55. Kurihara, T.; Matano, A.; Noda, Y.; Takegoshi, K., Rotational Motion of Ligand-Cysteine on CdSe Magic-Sized Clusters. *J. Phys. Chem. C* **2019,** *123* (24), 14993-14998.
56. Eliel, E. L.; Wilen, S. H., *Stereochemistry of organic compounds*. 1st ed.; Wiley-Interscience: New York, 1994; p 1296.
57. Romer, S.; Behzadi, B.; Fasel, R.; Ernst, K.-H., Homochiral Conglomerates and Racemic Crystals in Two Dimensions: Tartaric Acid on Cu(110). *Chem. Eur. J.* **2005,** *11* (14), 4149-4154.
58. Ortega Lorenzo, M.; Baddeley, C. J.; Muryn, C.; Raval, R., Extended surface chirality from supramolecular assemblies of adsorbed chiral molecules. *Nature* **2000,** *404* (6776), 376-379.
59. Haq, S.; Liu, N.; Humblot, V.; Jansen, A. P. J.; Raval, R., Drastic symmetry breaking in supramolecular organization of enantiomerically unbalanced monolayers at surfaces. *Nature Chem.* **2009,** *1* (5), 409-414.
60. Barlow, S. M.; Louafi, S.; Le Roux, D.; Williams, J.; Muryn, C.; Haq, S.; Raval, R., Supramolecular Assembly of Strongly Chemisorbed Size- and Shape-Defined Chiral Clusters: S- and R-Alanine on Cu(110). *Langmuir* **2004,** *20* (17), 7171-7176.
61. Zaera, F., Chirality in adsorption on solid surfaces. *Chem. Soc. Rev.* **2017,** *46* (23), 7374-7398.
62. Zhou, Y.; Yang, M.; Sun, K.; Tang, Z.; Kotov, N. A., Similar topological origin of chiral centers in organic and nanoscale inorganic structures: effect of stabilizer chirality on optical isomerism and growth of CdTe nanocrystals. *J. Am. Chem. Soc.* **2010,** *132* (17), 6006-6013.

63. Voelter, W.; Jung, G.; Breitmaier, E.; Bayer, E., 13C-Chemische Verschiebungen von Aminosäuren und Peptiden / 13C-NMR Chemical Shifts of Amino Acids and Peptides. *Z. Naturforsch. B* **1971,** *26* (3), 213-222.
64. Surprenant, H. L.; Sarneski, J. E.; Key, R. R.; Byrd, J. T.; Reilley, C. N., Carbon-13 NMR studies of amino acids: Chemical shifts, protonation shifts, microscopic protonation behavior. *J. Magn. Reson.* **1980,** *40* (2), 231-243.
65. Norris, D. J.; Bawendi, M. G., Measurement and assignment of the size-dependent optical spectrum in CdSe quantum dots. *Phys. Rev. B* **1996,** *53* (24), 16338-16346.

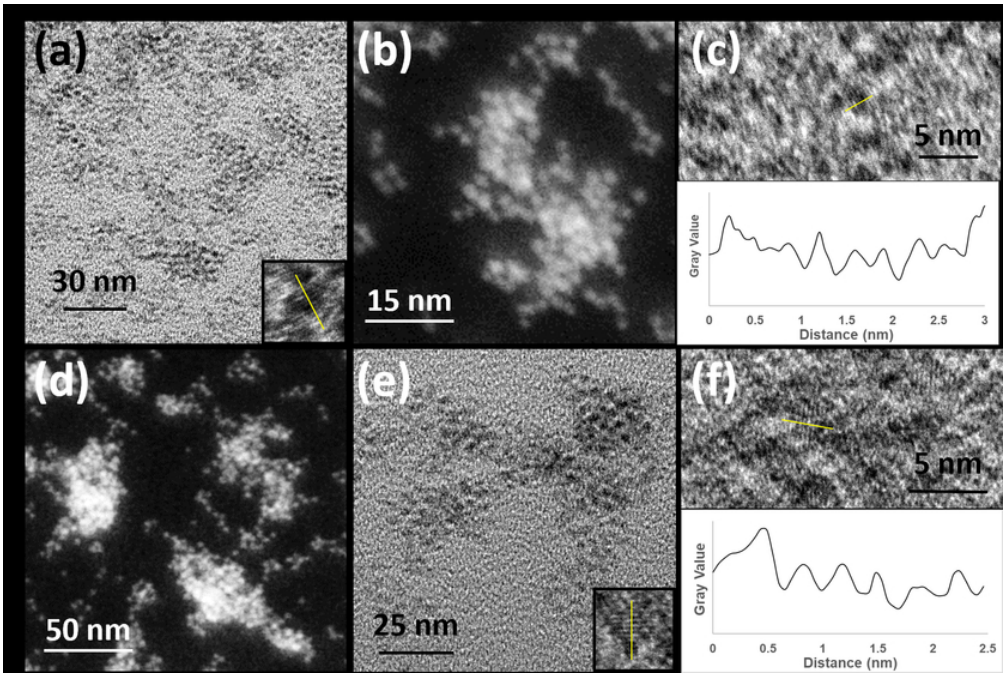

Figure 1. Brightfield TEM images, darkfield HAADF images, and the grey scale cross-sections of (a-c) L-Asp-CdS and (d-f) L-allo-Thr-CdS (ØCdS = 4.2 nm). Insets in (a) and (e): Images of QDs showing lattice fringes corresponding to CdS (100) crystal planes with spacing of ~3.37 Å (box size: ~5 × 5 nm).

70x47mm (300 x 300 DPI)

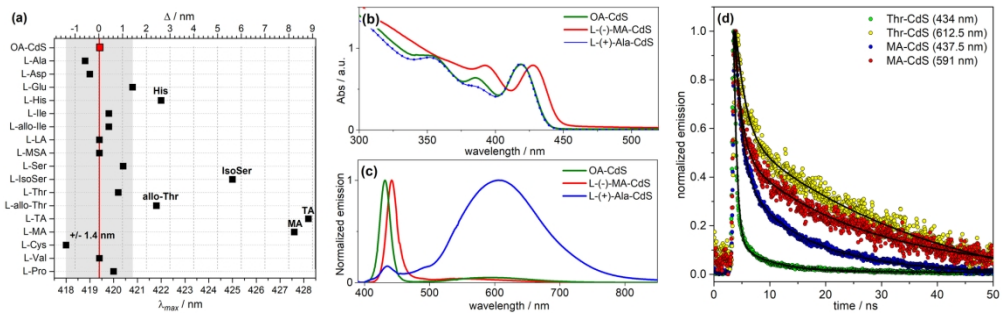

Figure 2. (a) Wavelength of the chiral CdS lowest energy excitonic peak as a function of the chiral carboxylic acid capping ligand in methanol (x-axis bottom) and the shift of the wavelength of the chiral CdS lowest energy excitonic peak relative to the OA-CdS in cyclohexane (Δλmax in nm, x-axis top). (b) UV-vis absorption and (c) normalized emission spectra (λexc = 355 nm) of OA-CdS, L-MA-CdS and L-Ala-CdS QDs in MeOH. (d) Band-edge (λem = 434 and 437.5 nm) and trap-state (λem = 612.5 and 591 nm) photoluminescence decays and their two-exponential fits for L-Thr-CdS and L-MA-CdS in MeOH.

179x56mm (300 x 300 DPI)

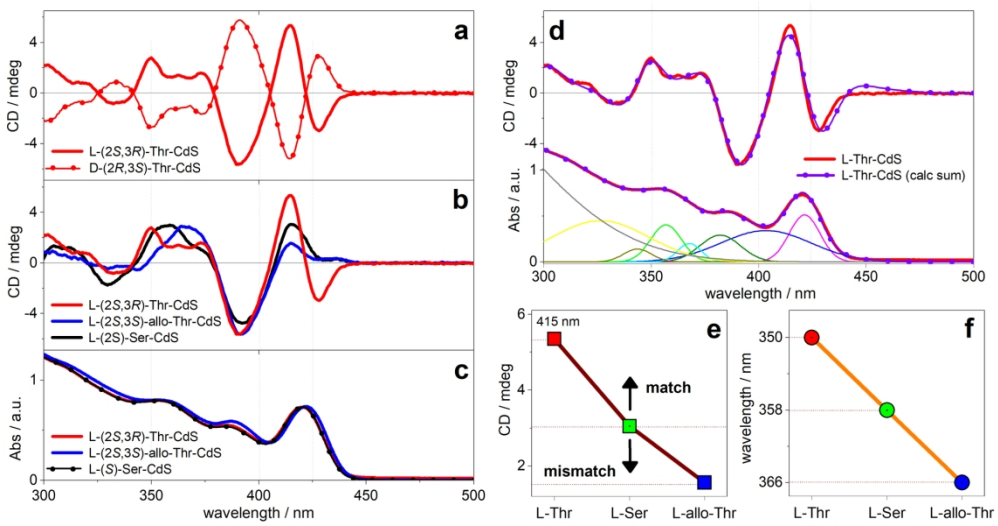

Figure 3. (a) CD spectra of L- and D-Trh-CdS. (b) CD and (c) UV-vis spectra of L-Thr-, L-allo-Thr-, and L-Ser-CdS; [CdS] ≈ 1.5 μM. (d) Simulated CD and UV-vis spectra of L-Thr-CdS. (e) CD intensity (415 nm) and (f) wavelength of the CD band (≈358 nm) of Ser-, Thr-, and allo-Thr-CdS. [CdS] ≈ 1.5 μM.

179x96mm (300 x 300 DPI)

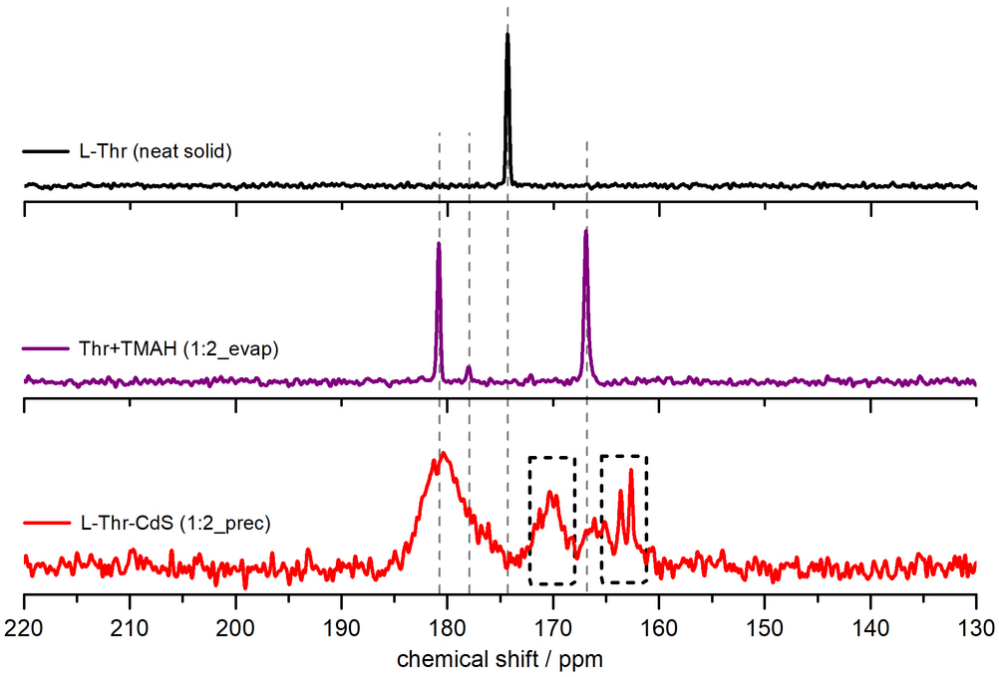

Caption : Figure 4. Carbonyl region of the 13C MAS ssNMR spectra of L-Thr-CdS. Black dashed rectangles encompass new signals in L-Thr-CdS QDs. Spectra were referenced to DSS (sodium salt of 2,2-dimethyl-2-silapentane-5-sulphonic acid). The spectra were acquired utilizing cross polarization from 1H to 13C, the areas under the signals are not necessarily proportional to the number of carbons, and the amount of each form cannot be determined quantitatively.

84x57mm (300 x 300 DPI)

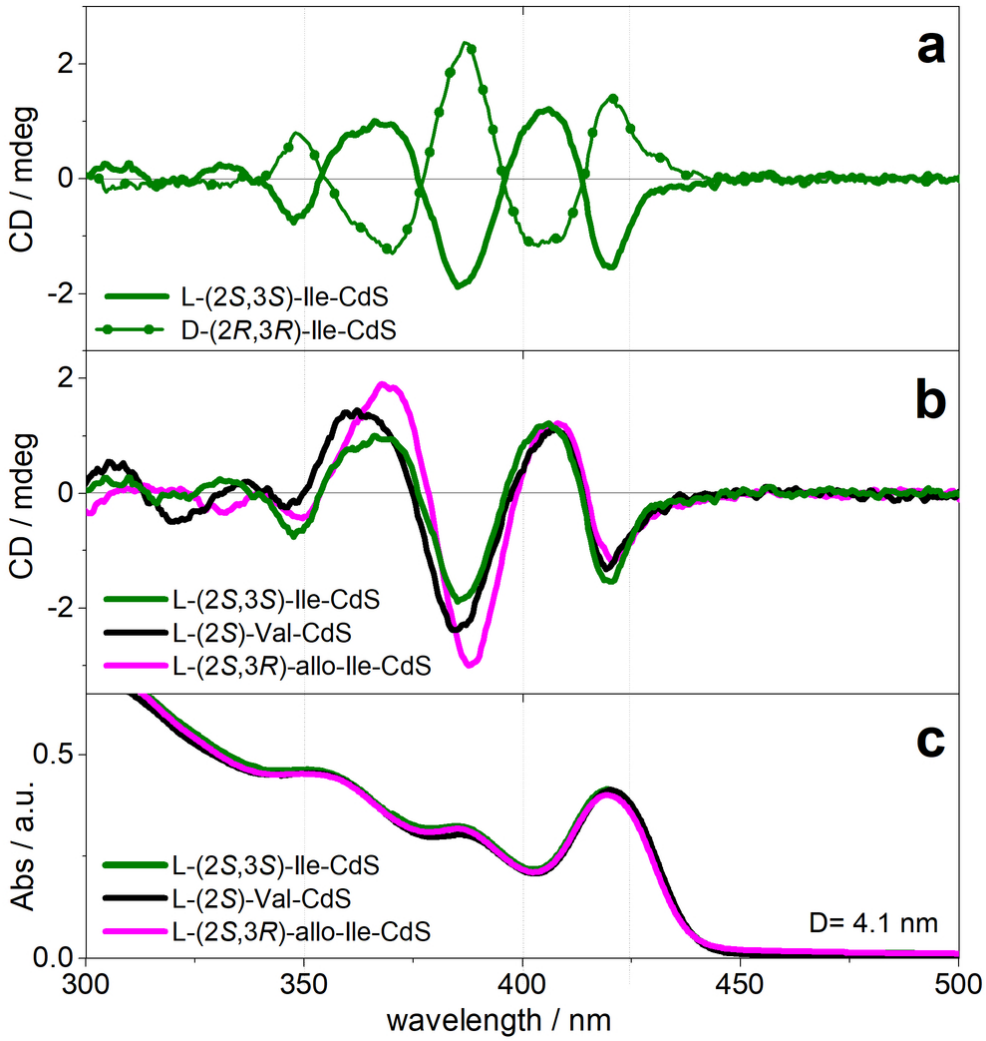

Figure 5. (a) CD spectra of L- and D-Ile-CdS; [CdS] ≈ 0.7 μM. (b) CD and (c) UV-vis spectra of Ile-, allo-Ile-, and Val-CdS; [CdS] ≈ 0.7 μM.

84x88mm (300 x 300 DPI)

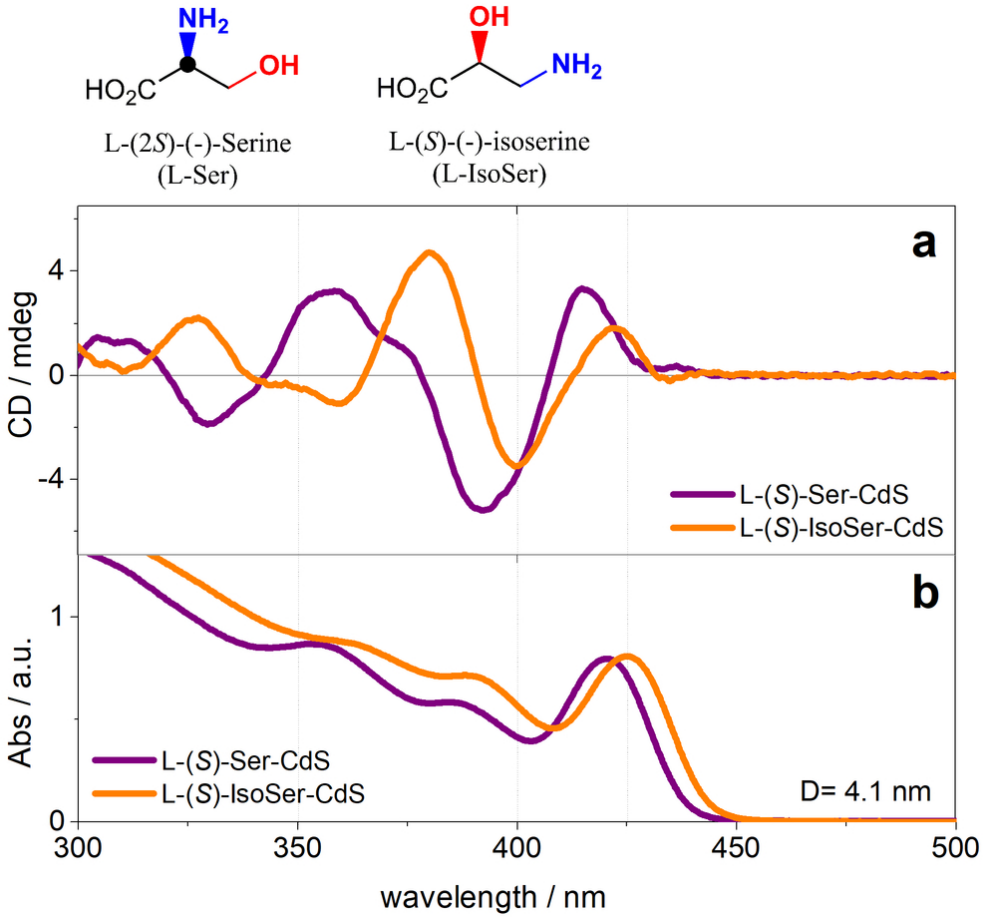

Figure 6. (a) CD and (b) UV-vis absorption spectra of L-Ser-CdS and L-IsoSer-CdS; [CdS] ≈ 1.5 μM.

84x80mm (300 x 300 DPI)

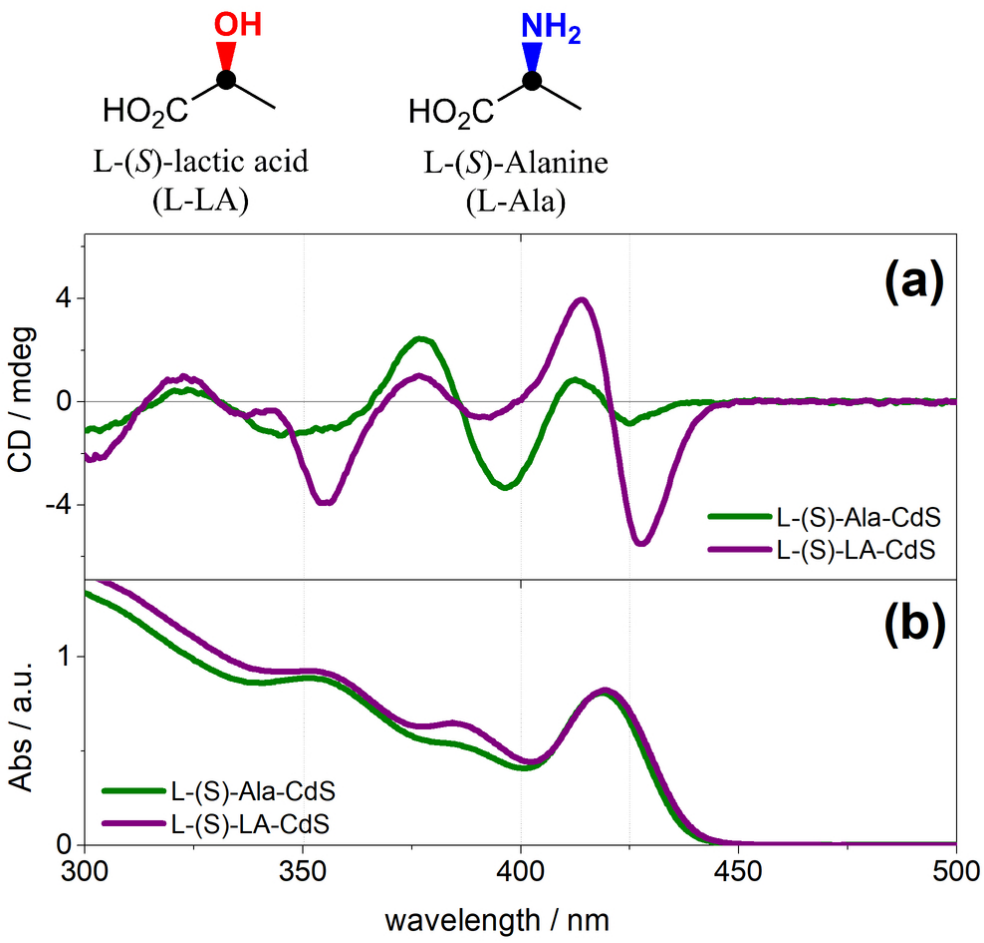

Figure 7. (a) CD and (b) UV-vis absorption spectra of L-Ala-CdS and L-LA-CdS; [CdS] ≈ 1.5 μM.

85x80mm (300 x 300 DPI)

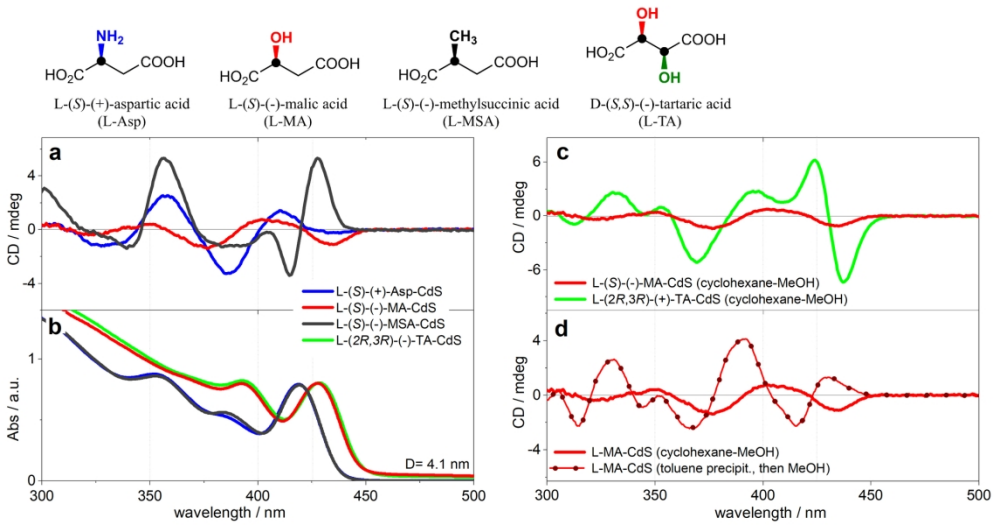

Figure 8. (a) CD and (b) UV-vis absorption spectra of L-Asp-CdS (blue curve), L-MA-CdS (red curve), and L-MSA-CdS (black curve) prepared by cyclohexane→MeOH ligand exchange; [CdS] ≈ 1.5 μM. (c) CD spectra of L-MA-CdS (red curve) and L-TA-CdS (green curve) prepared by cyclohexane→MeOH ligand exchange. (d) CD spectra of L-MA-CdS prepared by (i) cyclohexane→MeOH ligand exchange (red solid curve) and (ii) precipitated from toluene, then redissolved in MeOH (red dotted curve).

180x95mm (300 x 300 DPI)